Reduction of Tilt Suspension Force Pulsation and Interference in a 4-Pole 6-Slot Axial Maglev Motor

Nobuyuki KURITA *, Junichi ASAMA**, Victor TEDESCO ***,
Ethan MADDIN ***, Iki ADACHI *, and Yaxin WANG***
*Department of Surgery, Baylor College of Medicine
1 Baylor Plz, Houston, TX 77030 USA
Email: nobuyuki.kurita@bcm.edu
**Department of Mechanical Engineering, Shizuoka University, Japan
3 Chome-5-1 Johoku, Chuo Ward, Hamamatsu, Shizuoka 432-8011, Japan
*** Innovative Device & Engineering Applications Laboratory, Texas Heart Institute
6770 Bertner Ave, Houston, TX 77030 USA

Abstract
This study presents the design, control strategy, and experimental validation of a 4-pole, 6-slot axial-gap magnetically levitated motor intended for use in implantable artificial heart systems. The proposed motor integrates a permanent magnet stator and a maglev motor structure capable of actively controlling three degrees of freedom (axial and tilt directions), while achieving passive stabilization in the radial directions. To address the issue of tilt-direction suspension force pulsation and interference, a novel control method is introduced. This method employs a pseudo-inverse matrix derived from three-dimensional finite element method analysis to optimize the distribution of control currents and minimize force ripples.
The motor's structural and electromagnetic characteristics were analyzed, and its performance was evaluated through both static and dynamic experiments. Static force measurements confirmed that the axial suspension force can be balanced at a 1.5 mm air gap, enabling near-zero control current operation. Dynamic tests demonstrated stable levitation and rotation in both air and water environments, with improved damping and vibration suppression observed in water due to fluid viscosity. The system achieved stable operation up to 2000 rpm in water, while maintaining an experimentally verified controllable axial range of 0.67 mm.
These results validate the feasibility of the proposed maglev motor for artificial heart applications. Future work will focus on expanding the levitation range, refining tilt control gains, and redesigning the fluidic housing to incorporate a volute structure with inlet and outlet ports, thereby enabling higher rotational speeds and improved pressure generation suitable for physiological conditions.

Keywords: Maglev Motor, Suspension Force pulsation, Artificial Heart

1. Introduction

Cardiovascular disease, recognized as one of the three leading causes of death, accounts for about 15% of all deaths in Japan (Ministry of Health, Labor and Welfare, Japan, 2023) and nearly 30% in the United States (World Heart Federation, 2023). For patients with end-stage heart failure, heart transplantation remains the most effective treatment. However, the supply of donor hearts is critically limited. In Japan, the average waiting time for a heart transplant ranges from three to four years after registration (Japan Organ Transplant Network, 2025), while in the United States, although regional differences exist, approximately 49% of patients stay on the transplant waiting list for more than one year (Health Research Funding, 2025). To make life safer until a donor heart is found, Left Ventricular Assist Devices (LVADs) have been developed as a bridge-to-transplant option or as a long-term mechanical circulatory support system (Masuzawa, 2017). Among these, continuous-flow LVADs using magnetically levitated (Maglev) impellers have gained significant attention due to their potential to improve device longevity and eliminate contamination risks associated with mechanical bearings and lubricants (Hoshi, 2006, Schmitto, 2024). In Maglev LVADs, stabilizing five degrees of freedom (DOF)—

three translational (x, y, z) and two angular (θx, θy)—is crucial to ensure precise impeller positioning and reliable operation. Various approaches have been proposed to reduce system complexity and size, including passive stabilization of certain DOFs via magnetic coupling with permanent magnets or null-phase current through specialized winding configurations (Schoeb, 1997, Asama, 2015). Structurally, bearingless motors used in Maglev systems are categorized into radial-gap and axial-gap types. Additionally, based on the integration of magnetic bearing and motor functions, these systems are classified into (i) separated and (ii) magnetically integrated configurations (Chiba, 2005). The winding architecture of bearingless motors also broadly divides into (i) split winding types, with separate suspension and torque-generating windings, and (ii) integrated winding types, where both functions are achieved through superimposed currents (Khamitov, 2021, Raggl, 2007, Dietz, 2019). In this study, an axial-gap configuration is adopted to enable active control of axial displacement, counteracting fluid-induced axial forces in centrifugal pump applications. A three-DOF actively controlled bearingless motor with an integrated winding design is proposed to achieve system miniaturization and simplification (Kurita, 2015). Although several axial-gap bearingless motor designs have been previously reported (Masuzawa, 2017, Okamura, 2010, Ueno, 2022), this work introduces a novel structure that includes a permanent magnet-based magnetic coupling directly above the rotor within a three-DOF control framework. Additionally, a control method is proposed to reduce pulsations in the tilt-direction suspension force by superimposing harmonic components onto the support current. This approach addresses limitations seen in conventional current control methods. The effectiveness of the proposed method is validated through three-dimensional finite element electromagnetic analysis and confirmed by experimental results.

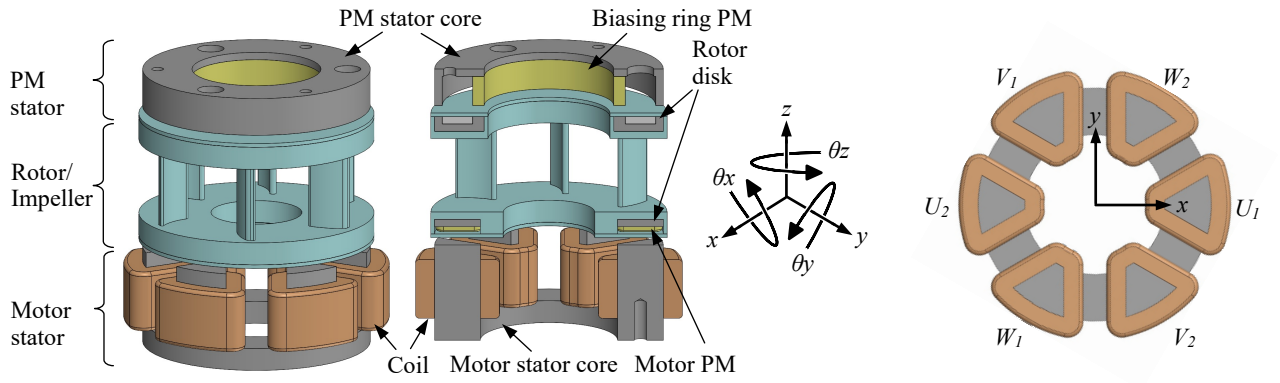

Figure 1: Schematic diagram of the experimental setup for a maglev motor. The left figure shows the overall view. The second figure from the left displays a cross-sectional view. This setup consists of an upper PM stator, a lower motor stator, and a rotor/impeller placed at the center. It is omitted in the figure, but the upper and lower stators are fixed together as a single unit. The rightmost figure is a schematic diagram of the motor stator viewed from the airgap side. The direction aligned with the U1 coil is the x-axis, and the direction of the center of the V1 and W2 coils is the y-axis.

2. Material and Methods

2.1 Proposed Maglev Motor

Figure 1 presents the structural configuration of the proposed axial-gap Maglev motor, designed for use in implantable blood pumps. The motor comprises a disk-shaped rotor positioned between two stators arranged vertically. The upper stator, referred to as the permanent magnet (PM) stator, consists of a magnetic core with a cylindrical shape and a closed top and an axially magnetized ring-shaped PM. This configuration forms a magnetic flux path with the ring-shaped core integrated into the rotor. The lower stator, termed the motor stator, is separated from the upper section by a non-magnetic disk spacer and adopts a 6-slot, 4-pole axial-gap motor topology. The motor rotor incorporates four PMs mounted on a disk-shaped magnetic back yoke, while the stator employs concentrated windings, with one coil wound around each tooth. Each of the six coils is independently energized.

The non-magnetic spacer region is designed to accommodate an impeller, enabling the motor to function as a centrifugal blood pump. A magnetic circuit forms between the PM stator and the rotor's ring-shaped core through the bias flux produced by the PM, causing an upward magnetic attraction force. At the same time, a downward magnetic force is generated by the bias flux in the axial-gap motor section. Although these opposing axial forces can be balanced

when static, the system remains magnetically unstable in three degrees of freedom—axial displacement (z-axis) and tilt (θx, θy)—requiring active control.

To stabilize axial movement, the suspension force along the z-axis is actively controlled by adjusting the d-axis current. That is, the axial suspension force is increased or decreased through field-strengthening or field-weakening control. Rotor torque is controlled separately via the q-axis current. In this maglev motor, the six stator coils are controlled independently to create a four-pole rotating magnetic field, which generates rotating torque and enables axial force control. When the rotor and stator surfaces are parallel, no net torque occurs in the tilt direction. However, if the rotor tilts, the asymmetry in air gap width causes a differential magnetic flux density—dense on the narrower side and sparse in the broader side—leading to an unbalanced torque aligned with the tilt. This inherent instability requires closed-loop feedback control based on tilt displacement measurements. A two-pole rotating magnetic field is superimposed on a four-pole rotating magnetic field to produce suspension forces in the tilt directions (θx, θy), enabling active stabilization through tilt control torque.

The principle of passive radial suspension in the proposed motor is based on the attractive force in the axial direction (z). The bias magnetic flux generated by the PM stator and the motor rotor PMs establishes a magnetic coupling between the stator and rotor. When the rotor experiences a radial displacement, the resulting asymmetry in magnetic reluctance induces a restoring force directed toward the equilibrium position, where the magnetic reluctance is minimized. This restoring force enables passive stabilization of the rotor in the radial directions (x and y), eliminating the need for active control in these two degrees of freedom.

2.2 Tilt support force ripple reduction control

As illustrated in Figure 1, the stator coils are labeled U_1, W_2, V_1, U_2, W_1, and V_2 in a counterclockwise arrangement, with U_1 aligned along the x-axis. The direction of current that produces a north magnetic pole in the air gap is defined as positive, as indicated by the dashed arrow in the lower-right diagram of Figure 1. Let the target suspension currents for each phase be denoted as i_{utr}, i_{vtr}, i_{wtr}, and the target suspension forces in the tilt directions around the x- and y-axes be $T_{\theta xr}$ and $T_{\theta yr}$, respectively. Under conventional control schemes, the relationship between these currents and forces is expressed as a function of the rotor's electrical angle θ_e.

$$\begin{bmatrix} i_{utr} \\ i_{vtr} \\ i_{wtr} \end{bmatrix} = \frac{1}{K_\theta}\sqrt{\frac{2}{3}}\begin{bmatrix} \sin\theta_e & -\cos\theta_e \\ \sin\left(\theta_e - \frac{2\pi}{3}\right) & -\cos\left(\theta_e - \frac{2\pi}{3}\right) \\ \sin\left(\theta_e - \frac{4\pi}{3}\right) & -\cos\left(\theta_e - \frac{4\pi}{3}\right) \end{bmatrix}\begin{bmatrix} T_{\theta xr} \\ T_{\theta yr} \end{bmatrix} \tag{1}$$

Let K_θ denote the tilt suspension force coefficient. The electrical angle $\theta_e = 0$ is defined as the position where the rotor's north magnetic pole is aligned with the U_1 coil. The left-hand side of equation (1) represents the current distribution responsible for generating a two-pole magnetic field. For instance, in the U-phase, a current $\boldsymbol{i_{utr}}$ is applied to the U_1 coil, while a current of $-i_{utr}$ is simultaneously applied to the U_2. However, when this conventional control method, as described by equation (1), is employed, pulsations are observed in the actual tilt-direction suspension force.

To address this issue, we suggest an enhanced control strategy that utilizes Silber and Amrhein's (Silber, 2000) control current optimization method for tilt support force control and determines the force coefficient as a function of the rotor electrical angle through three-dimensional finite element method (3D FEM) analysis. Based on these computed coefficients, the target suspension currents are determined by solving a pseudo-inverse matrix problem, thereby minimizing the pulsation in the tilt-direction suspension force.

Assuming that radial displacement is negligible, the tilt-direction suspension force vector $\boldsymbol{Q}$ and the corresponding suspension current vector i_t can be represented as follows:

$$\boldsymbol{Q} = \begin{bmatrix} \boldsymbol{T_{\theta x}} \\ \boldsymbol{T_{\theta y}} \end{bmatrix} = \boldsymbol{K}(\theta_e)\begin{bmatrix} i_{u1t} \\ i_{v1t} \\ i_{w1t} \\ i_{u2t} \\ i_{v2t} \\ i_{w2t} \end{bmatrix} = \boldsymbol{K}(\theta_e)\boldsymbol{i_t} \tag{2}$$

The matrix $\boldsymbol{K}(\theta_e)$ represents the force coefficient matrix, where each element is a function of the rotor's electrical angle θ_e. The tilt suspension force is calculated using 3D FEM magnetic field analysis, with the rotor's electrical angle θ_e varied from 0° to 360°. During this process, a control current of 1 A is applied to the U_1 coil. The force-angle relationship derived from this analysis is then used to determine the corresponding component of the force coefficient matrix $\boldsymbol{K}(\theta_e)$ for the U_1 coil through curve fitting. This procedure is systematically repeated for each of the six stator coils, and the complete matrix $\boldsymbol{K}(\theta_e)$ is constructed by combining the fitted results. Since $\boldsymbol{K}(\theta_e)$ is a non-square matrix, its inverse cannot be directly computed. Therefore, a pseudo-inverse matrix $\boldsymbol{K}(\theta_e)$ is employed to determine the suspension current vector that minimizes the Euclidean norm of the current. This relationship can be expressed as follows:

$$\boldsymbol{i_t} = \boldsymbol{K_p}(\theta_e)\boldsymbol{Q} = \boldsymbol{K}^T(\boldsymbol{K}\boldsymbol{K}^T)^{-1}\boldsymbol{Q} \tag{3}$$

The computed pseudo-inverse matrix is substituted into equation (3) to obtain the control current vector. This control current is designed to minimize both the pulsation and mutual interference components of the tilt-direction suspension

force, thereby enhancing the stability and precision of the levitation control system. A more detailed explanation of this method, including the results of the three-dimensional magnetic field analysis, is provided in the reference (Kurita, 2025).

2.3 Static force measurement method

To minimize the control current required during steady-state operation, the reference position of the magnetically levitated rotor is defined as the equilibrium point at which the attractive forces generated by the upper PM stator and the lower motor-side PM are balanced. Accurate determination of this equilibrium condition necessitates precise measurement of the static suspension force. To facilitate this, a dedicated static force measurement apparatus was designed and constructed. A photograph of the experimental setup is provided in Figure 2. The experimental setup includes a high-resolution force transducer (ATI Industrial Automation, NC, USA) with a resolution of 1/512 N, mounted on a micrometer-driven XYZ stage (MiSUMi, Inc., Japan). The motor under test is attached to the force transducer so that the rotor's permanent magnet hangs directly above the stator. The axial gap between the rotor and stator is precisely adjustable through a linear stage. Additionally, the motor windings are connected to current amplifiers, allowing for adjustments to the suspension current flowing through each coil. Data collection was performed using a custom LabVIEW program connected to an NI 4212 data acquisition module (National Instruments, TX, USA). The LabVIEW script was set to record individual force measurements at specific axial gap positions and control current. The support force of the PM stator is measured in a similar way.

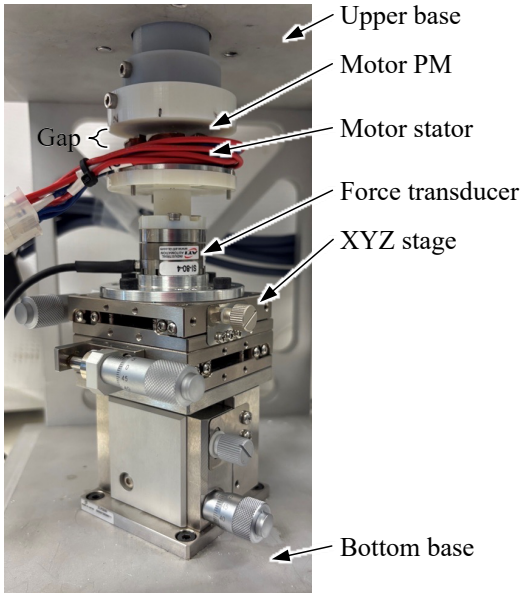

Figure 2 Photo of the static force test rig.

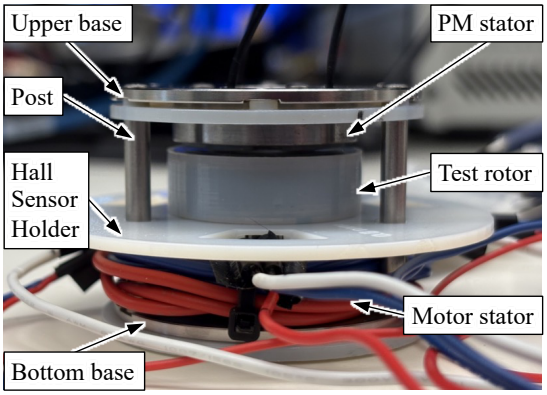

Figure 3 Photo of the dynamic test rig of the maglev motor.

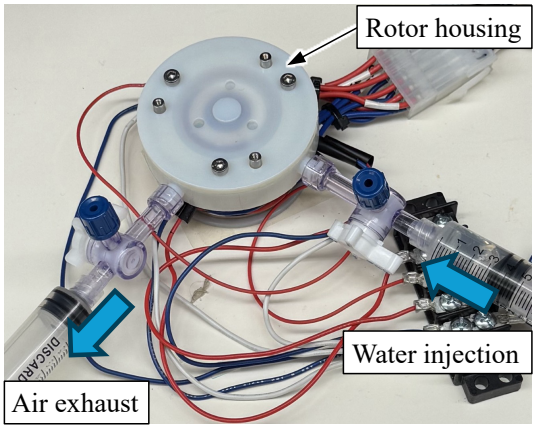

Figure 4 Photo of the experimental setup for the dynamic tesing in the water.

Axial force measurements were taken across an airgap ranging from 1.0 mm to 2.0 mm between the stator and rotor, with increments of 0.1 mm. For each gap, the control current varied from −2.5 A to +2.5 A in 0.5 A increments. The same measurement process was used to assess the axial force between the rotor disk and the upper PM stator. The upper and lower limits of the control current are set to ±2.5A to prevent the coil from overheating.

2.4 Vibration measurement method

Figure 3 illustrates the dynamic test setup designed to assess the levitation and rotation capabilities of the maglev motor. The setup includes a rigid upper and lower base, which hold the upper permanent magnet (PM) stator and the motor stator, respectively. These bases are supported by three vertical posts. A 3D-printed fixture is mounted above the motor stator to hold a Hall-effect sensor that detects the rotor's angular position. Although not visible in the photograph, eddy current displacement sensors are embedded within the upper PM stator to monitor axial movement. By adjusting the current supplied to the motor windings, the magnetic field distribution is changed, allowing precise control of the airgap between the rotor and both the upper and lower stators. The dynamic behavior of the system was examined by measuring the vibration amplitude of the levitated rotor at different rotational speeds, in both air and water. Figure 4 presents the experimental setup used to investigate the system's dynamic characteristics in a water-immersed environment (the upper PM stator was removed to enable observation). The rotor assembly was enclosed in a 3D-printed housing, filled with water. One syringe introduced water while the other evacuated air simultaneously to ensure complete filling without air pockets.

3. Results

3.1 Static force measurement result

Figure 5 shows the measurement results of the static attractive force along the axial direction. The rotor's allowable displacement range on the z-axis is 3 mm. The horizontal axis of the graph defines the axial gap as 0 mm when the rotor is in direct contact with the motor stator. A 1 mm gap means there is a 1 mm separation between the rotor and the motor stator, implying a gap of 2 mm between the rotor and the upper PM stator. Conversely, a 2 mm gap indicates a 2 mm separation from the motor and a 1 mm gap from the PM stator. In the legend, the curves labeled from −2.5 A to +2.5 A represent the attractive force generated by the motor stator under different control current conditions. As expected, the attractive force increases as the airgap narrows and decreases as the gap widens. Additionally, the magnitude of the attractive force can be adjusted by changing the control current. The curve labeled "PM stator" in the legend corresponds to the attractive force produced by the PM in the upper PM stator. Since the PM stator contains no electromagnetic components, its attractive force depends solely on the airgap. The attractive force decreases as the gap on the PM stator side increases (i.e., as the rotor moves downward), and increases as the gap narrows (i.e., as the rotor moves upward). It was observed that when both the motor and PM stator gaps are equal at 1.5 mm, the attractive forces generated by the motor (at 0 A control current) and the PM stator are approximately 10.5 N each. At this equilibrium point, the net axial force is balanced, enabling levitation control with a near-zero control current. Furthermore, when the rotor moves downward, reducing the motor-side gap to 1.1 mm, it can be restored to its equilibrium position by applying a negative control current of −2.5 A. This current reduces the motor-side attractive force, allowing the stronger force from the PM stator to "pull" the rotor upward. Conversely, when the rotor moves upward and the motor-side gap widens to 1.77 mm, applying a +2.5 A control current increases the motor-side attractive force, causing the rotor to "pull" back downward. These findings suggest that the effective controllable axial rotor range is approximately 0.67 mm.

This maglev motor is intended for application in implantable artificial heart systems. Accordingly, the rotor impeller must be encapsulated within a biocompatible titanium casing, and the stator must likewise be enclosed in a titanium housing. Additionally, to minimize hemolysis and ensure safe blood flow, the target clearance for the blood flow channel is set to 0.5 mm. Assuming that both the rotor and stator are covered with titanium layers of 0.5 mm thickness, the required mechanical air gap between the rotor and each stator surface must be 1.5 mm to maintain the desired 0.5 mm fluid gap. Given that the rotor must accommodate axial displacement of ±0.5 mm (i.e., a total stroke of 1.0 mm), the magnetic suspension system must support this range of motion. At present, the experimentally verified controllable axial displacement range is limited to approximately 0.67 mm. This range may be extended by either (i) reducing the stiffness (i.e., the gradient) of the attractive force generated by the upper PM stator or (ii) increasing the magnitude of the control

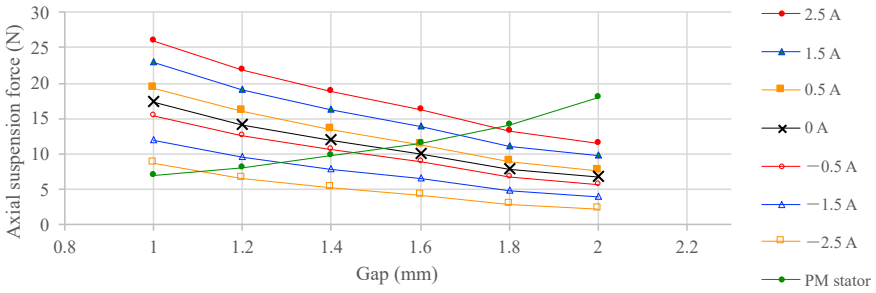

Figure 5 Static attractive force measurement result.

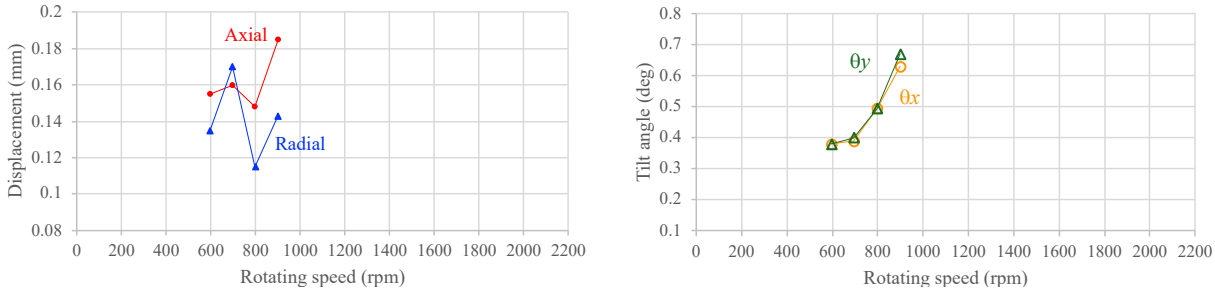

Figure 6 Vibration amplitude versus rotating speed in air

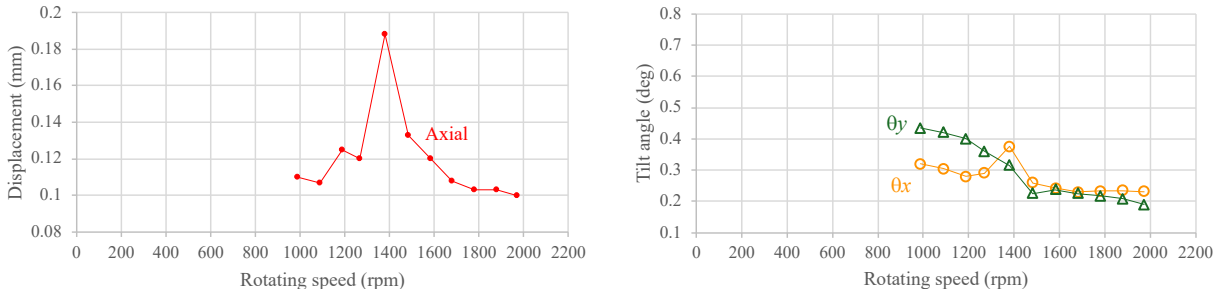

Figure 7 Vibration amplitude versus rotating speed in water

current applied to the motor windings. Magnetic field simulations indicate that a control current of approximately ±5 A applied for 0.5 seconds is sufficient to achieve the required force modulation. Future work will investigate both strategies to expand the effective levitation range, thereby satisfying the mechanical and physiological constraints imposed by artificial heart applications.

3.2 Vibration amplitude measurement result

Figure 6 and 7 shows results of vibration amplitude measurements under dynamic magnetic levitation conditions. Figure 6 presents the results obtained in air, while Figure 7 shows those acquired in water. In the experiments conducted in air, radial displacement was measured using a laser displacement sensor. Conversely, during tests in water, the rotor was enclosed within a sealed housing, which prevented the use of laser displacement measurements. Magnetic levitation control was mainly implemented through the current distribution method described in Section 2.2, which includes a tilt force ripple suppression technique. The conventional control method based on Equation (1) was also tested. However, stable levitation could not be achieved with this method due to radial interference forces occurring during tilt control. Therefore, all reported data were obtained using the control strategy outlined in Section 2.2.

In air, stable levitation and rotational control were achieved within a speed range of 550 to 900 rpm. Axial position control remained stable across all tested speeds. However, due to the low stiffness associated with passive radial stabilization, radial vibrations of approximately 0.1 mm amplitude were consistently observed. Measurements of tilt control indicated that the tilt angle increased with rotational speed, reaching about 0.5 degrees at 900 rpm. The control system was ultimately stopped, likely because of excessive vibration amplitude during tilt control. This issue could potentially be addressed in future work by optimizing the tilt control gain.

Experiments in water showed improved stability, with successful levitation and rotation maintained over a speed

range of 1000 to 2000 rpm. This improvement is mainly attributed to the damping effects of water viscosity. Notably, the axial vibration amplitude increased near 1400 rpm, possibly corresponding to the natural frequency of the passively stabilized radial mode. Water's damping also reduced vibration amplitude in the tilt direction. However, the sealed housing used during underwater tests was not designed to withstand pressure-induced forces generated during rotor rotation. These unbalanced pressure distributions may have acted as load torques, potentially causing the rotor to decelerate or stop. To investigate this further, future experiments will include real-time monitoring of the motor's control current to identify and analyze such disturbances. To achieve higher rotational speeds and better pressure management, future designs will replace the simple enclosure with a volute-shaped housing that includes inlet and outlet ports. This modification is expected to facilitate appropriate pressure buildup during operation and enhance the motor's performance in fluid environments.

4. Conclusion

This study proposed and experimentally validated a control strategy to reduce tilt-direction suspension force pulsation and interference in a 4-pole, 6-slot axial-gap magnetically levitated motor designed for artificial heart applications. By introducing a current distribution method based on a pseudo-inverse matrix derived from three-dimensional finite element analysis, the approach effectively minimized force ripple and enhanced levitation stability.

The motor structure, which combines a PM stator with an actively controlled three-degree-of-freedom maglev motor, demonstrated stable levitation and rotation in both air and water environments. Static force measurements confirmed that the axial suspension force could be balanced at a 1.5 mm air gap, enabling near-zero control current operation. The experimentally verified controllable axial range of 0.67 mm, although currently limited, is sufficient for basic levitation control and can be extended through design optimization or increased control current. Specifically, dynamic testing demonstrated that water's damping effect greatly enhanced dynamic stability, enabling operation up to 2000 rpm.

These findings support the feasibility of the proposed maglev motor design for use in implantable blood pumps. Future research will focus on expanding the controllable levitation range, optimizing tilt control gains, and redesigning the fluidic housing to incorporate a volute structure with inlet and outlet ports, which will enable higher rotational speeds and better pressure generation suitable for physiological conditions.

References

Asama, J., et al.: “Novel Control Method for Magnetic Suspension and Motor Drive with One Three-Phase Voltage Source Inverter Using Zero-Phase Current”, Mechanical Engineering Journal, Vol. 2, No. 4, Paper No. 15-00116 (2015)

Chiba, A., Fukao, T., et al., “Magnetic Bearings and Bearingless Drives”, Elsevier (2005)

Dietz, D., Binder, A., “Comparison between a bearingless PM motor with separated and combined winding for torque and lateral force generation”, Proceedings of the 21st European Conference on Power Electronics and Applications (2019)

Health Research Funding, “24 Important Heart Transplant Waiting List Statistics,” https://healthresearchfunding.org/

Hoshi, H., Shinshi, T., Takatani, S.: “Third-generation Blood Pumps with Mechanical Noncontact Magnetic Bearings”, Artificial Organs, Vol. 30, No. 5, pp. 324-338 (2006)

Japan Organ Transplant Network, “Waiting Periods for Transplant Applicants,” https://www.jotnw.or.jp/explanation/07/05/

Khamitov, A., et al., “Comparison of Combined Winding Strategies for Radial Nonsalient Bearingless Machines”, IEEE Transactions on Industry Applications, Vol. 57, No. 6, pp. 6856-6869 (2021)

Kurita, N., et al., “Proposal of a Permanent Magnet Hybrid-type Axial Magnetically Levitated Motor”, IEEJ Journal of Industry Applications, Vol. 4, No. 4, pp. 339-3415 (2015)

Kurita, Nobuyuki, Asama, Junichi, et. al., “Suspension Force Ripple Reduction Control of a Magnetically Levitated Axial Gap Bearingless Motor,” The proceedings of the IEMDC 2025, Paper No. 7119, Houston TX, (2025)

Masuzawa, Toru: “Magnetically Suspended Blood Pump,” Journal of the Japan Society of Applied Electromagnetics, Vol. 25, No. 3, pp. 22-33 (2017)

Ministry of Health, Labor and Welfare, Japan, “Overview of Demographic Statistics of 2022,” September 2023.

Mori, K., Asama, J., et al.; “Resonance avoidance for a 2-DOF controlled maglev motor using d-axis current”, Transactions of the JSME, Vol. 85, No. 872, 18-00417 (2019)
Okamura, T., Ueno, S., et. al., "Efficiency of Small Regenerative Pump Using Axial Self-Bearing Motor," Journal of the Japan Society of Mechanical Engineers (C) Vol. 76, No. 772, pp 3535-3541 (2010)
Raggl, K., Kolar, J. W., and Nussbaumer, T., “Comparison of Winding Concepts for Bearingless Pump”, Proceedings of the 7th International Conference on Power Electronics, pp. 1013-1020 (2007)
Schmitto, Jan D., Shaw, Steven, Garbade, Jens, et.al., “Fully magnetically centrifugal left ventricular assist device and long-term outcomes: the ELEVATE registry,” European Heart Journal, Volume 45, Issue 8, 21 February 2024, Pages 613–625, doi.org/10.1093/eurheartj/ehad658.
Schoeb, R., Barletta, N.: “Principle and Application of a Bearingless Slice Motor”, JSME International Journal, Series C, Vol. 40, No. 4 (1997)
Takeshi, S., et al.: “Development of a Disposable Maglev Centrifugal Blood Pump Intended for One-Month Support in Bridge-to-Bridge Applications: In-Vitro and Initial I-Vitro Evaluation”, Artificial Organs, Vol. 33, No. 9, pp. 704-713 (2009)
Ueno, S., et.al, "Development of Five-Axis Active Controlled Axial-Flux Self-Bearing Motor using Unipolar Magnetic Field," Journal of Japan AEM Society, Vol. 30, No. 2, pp. 79-85, (2022)
World Heart Report 2023, “Confronting the World’s Number One Killer,” Geneva, Switzerland. World Heart Federation, 2023.